applied optics

Large numerical aperture off-axis reflective telescope design with a freeform mirror based on aperture expansion strategy

JIALUN ZHANG,[1] YUQUAN ZHENG,[1,*] CHAO LIN,[1] YANXUE HAN,[1,2] AND YI SHI[1,2]

[1]Changchun Institute of Optics, Fine Mechanics and Physics, Chinese Academy of Sciences, Changchun 130033, China
[2]University of Chinese Academy of Sciences, Beijing 100049, China
*zhengyq@sklao.ac.cn

Received 4 November 2022; revised 13 January 2023; accepted 18 January 2023; posted 20 January 2023; published 13 February 2023

Currently, the emission of greenhouse gases is one of humanity's leading threats. To accurately and efficiently measure greenhouse gas levels in the atmosphere, we must develop imaging spectrometer systems with larger numerical apertures (NAs). However, designing a telescope with a large NA is difficult in this system. This paper presents a design strategy for aperture expansion to create a freeform telescope with a large NA. We compared different off-axis reflective telescopes and chose the Korsch structure, which has obvious advantages because of its wide field of view (FoV), large NA, and low stray light. Moreover, based on the influence of the position of the freeform surface in the aberration correction, we propose to use a single freeform surface to reduce the cost and increase manufacturability. A freeform telescope with an effective focal length of 84 mm, a large NA of 0.25, and a wide FoV of 20° is successfully designed. The modulation transfer function of the system is better than 0.62, the maximum distortion is controlled to be less than 0.486%, and the incident angle of the beam on the image plane is less than 10°. The design result shows that the instrument has wide FoV, large NA, low stray light, and high performance. At the same time, the design strategy in this paper provides an effective method for the telescope design of the imaging spectrometer with a large NA.

https://doi.org/10.1364/AO.479862

1. INTRODUCTION

Under the framework of the Paris Conference, major countries in the world have developed corresponding measurement programs to reduce greenhouse gas emissions. Among these measures, the imaging spectrometer is one of the most important satellite monitoring instruments for greenhouse gases. Within the Copernicus mission, the CO_2 monitoring (CO2M) mission was proposed by the European Space Agency (ESA) to enable rapid monitoring of global greenhouse gases [1]. The National Aeronautics and Space Administration (NASA) launched two satellites, OCO-2 and OCO-3, in 2014 and 2019, to enhance the monitoring capabilities of global greenhouse gases [2,3]. In addition, the Japan Aerospace Exploration Agency (JAXA) pushed out the GOSAT-2 satellite in 2018, providing larger detection accuracy and spatial sampling frequency than before [4]. Moreover, in 2016, China launched the TanSat, realizing the first space-based acquisition of global CO_2 data [5]. Now, to serve the double carbon policy of the Chinese government, China is planning to develop the next generation of TanSat. The new generation of imaging spectrometers requires larger spatial resolution and numerical aperture (NA) than its predecessors. The telescope of the imaging spectrometer is one of the essential components of the instrument, and the project plans to develop a telescope with a wide field of view (FoV) and a large NA. There is no doubt that the telescope of the imaging spectrometer was difficult in the development of this complex scientific instrument.

Traditional design methods are challenging to solve this problem effectively. In recent years, the rapid development of freeform surface optical technology has provided an opportunity to solve this problem. With the development of freeform surface testing and manufacturing technology, freeform surfaces have been successfully used in aerospace remote sensing instruments. In 2012, Nijkerk *et al.* introduced an anamorphic telescope system developed and designed for the Sentinel-5p instrument [6]. The telescope has an ultrawide FoV of over 108 , and the sagittal focal length is twice the meridional focal length. Without reducing the spatial resolution, the instrument has the ability to double the spectral sampling, which can improve spectral retrieval accuracy. The two concave mirrors of the telescope are both freeform mirrors, which can make the focus in the tangential and sagittal directions different and correct the severe aberrations caused by the large FoV. In 2015, Beier *et al*. introduced the design and manufacture of the telescope used in the IR Limb Sounder (IRLS) [7]. The multidegree freedom

of the freeform surface enables different magnifications in tangential and sagittal directions. The entrance pupil of the optical system is rectangular, while the exit pupil is square. In 2018, the off-axis four-mirror telescope with the freeform surface developed by Xin *et al*. was successfully launched with the GF-6 satellite [8]. The telescope has a wide FoV of 76°. The system has the characteristics of high imaging quality, small size, and light weight, relying on the excellent aberration correction ability of the freeform surface. In addition, many researchers worldwide have conducted a great deal of research on the design methods, testing, and manufacturing technologies of the freeform surface, which have made significant contributions to the successful application of the freeform surface [9–15].

The aforementioned research results show that the freeform surface has apparent advantages in designing the instrument with a wide FoV [16]. However, the design proposed in this paper is an entirely new challenge. We need the instrument to have a wide FoV and a very large NA and special requirements for parameters such as the entrance pupil. In this paper, based on solid research background, we analyze the different structural forms of the telescope. And the Korsch form is selected as the basic structure, which has obvious advantages in terms of the wide FoV, large NA, and low stray light [17–19]. According to the relationship between the freeform surface and aberration correction, we choose the appropriate position of the freeform surface, when there is only one freeform surface in the design. In addition, for the design problem of the off-axis reflective telescope with a large NA, we propose a strategy of aperture expansion, which can effectively reduce the design difficulty of such optical systems. Based on the analysis and design method in this paper, a compact off-axis three-mirror telescope with a freeform mirror is designed. The telescope consists of two low-order aspheric mirrors and a freeform mirror. The stop is in front of the primary mirror and coincides with the position of the entrance pupil. There is a real image plane between the primary and secondary mirrors, which has excellent stray light suppression capability. The telescope has a spectral range of 0.4–2.5 μm, F-number of 2, FoV of 20°, an effective focal length of 84 mm, an incident angle of the chief ray in the focal plane of less than 10°, and the length of the telescope is less than 310 mm. The freeform mirror plays a vital role in the design of the telescope. The freeform telescope designed in this paper is compact and has a wide field, large NA, and high performance.

2. ANALYSIS AND DESIGN METHODS OF THE TELESCOPE FOR THE IMAGING SPECTROMETER

Since the Industrial Age, a large amount of fossil fuel combustion, which caused the substantial increase in the content of CO_2, NO_2, CH_4, and SO_2, ha been the main reason for global warming. Among them, CO_2 is the most significant greenhouse gas. Monitoring global CO_2 emissions can lead to more rational national environmental protection policies. Currently, the leading bands for monitoring CO_2 are 1.595–1.675 μm and 1.990–2.095 μm. Because CO_2 is a natural and well-mixed constituent of Earth's atmosphere, its quantitative measurement is a challenge. Even though the content of CO_2 in the atmosphere has increased significantly today, it still occupies a meager percentage that is not conducive to discovery. The enhanced concentrations from industrial emissions are on the order of only a few percent of the background concentration. Fortunately, the emission sources are frequently accompanied by co-emitted nitrogen dioxide (NO_2), which has strong absorption in the 0.405–0.49 μm range. NO_2 can therefore be used as a tracer for CO_2 emission. Therefore, such a scientific instrument for monitoring CO_2 emissions should consist of multiple spectrometer subsystems. The telescope that provides light collection for these subsystems should be a wide spectrum optical system covering visible-near-infrared (VNIR) to shortwave-infrared (SWIR) (0.4–2.5 μm) [20]. At the same time, the telescope requires a stronger light-gathering capability and a wider FoV in order to improve the signal-to-noise ratio and spatial resolution of the imaging spectrometer. In this paper, the specifications of the telescope we designed are shown in Table 1.

Table 1. Specifications of the Telescope of the Imaging Spectrometer

Parameters	Value	Units
Orbit altitude	750	Km
Swath width	250	km
FoV	20	degree
F-number	2	-
Spectral range	0.4–2.5	mm
Spatial resolution	2 × 2	km
Focal length	84	mm
Detector pixel size	11 × 11 (VNIR); 30 × 30 (SWIR)	μm

A. Analysis of the Structural Form of the Telescope

For a long time, imaging spectrometers have been widely studied [9,10,21]. However, little thematic research has been done on telescopes for imaging spectrometers. In fact, the telescope is an integral part of an imaging spectrometer, which includes several typical structural forms such as refraction, on-axis or off-axis reflection, and catadioptric telescopes. Many research results show that off-axis reflective telescopes have more advantages in the wide spectrum and field. According to the specifications in Table 1, there is no doubt that the off-axis reflective telescope is the optimal structural form, even if the design needs to have a large NA. In this paper, the characteristics of various off-axis reflective telescopes are analyzed as follows.

1. Off-Axis Two-Mirror Telescope

There are three types of optical structures in the off-axis two-mirror telescope, as shown in Fig. 1. Both reflective mirrors are concave in Fig. 1(a), which is designed as an off-axis Gregory telescope. When the stop is at the focus of the secondary mirror, a telecentric result can be obtained. A real entrance pupil is formed in front of the primary mirror. In addition, the intermediate image plane between the primary and secondary mirrors is beneficial to install the field-limiting aperture (aperture stop). Nevertheless, with this structural form, it is difficult to obtain large NA, and so it is often used in designs with low

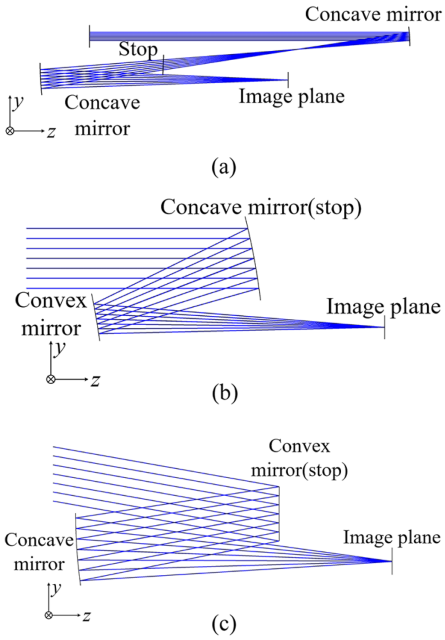

Fig. 1. Off-axis two-mirror telescope scheme of (a) two concave mirrors, (b) concave mirror and convex mirror, (c) convex mirror and concave mirror.

NA. An example of a successful application is the telescope of TROPOMI [6].

In Fig. 1(b), the optical elements are a concave mirror and a convex mirror, respectively. This is an off-axis Cassegrain telescope, and the stop can be placed anywhere. However, this structural form does not have an intermediate image plane, so it is difficult to set up a field-limiting aperture, and the problem of stray light is serious. In addition, when the NA of the telescope is large, the system has a large amount of the decenter or tilt, and aberration correction is complex.

By reversing the positions of the optical elements in Fig. 1(b), the structural form in Fig. 1(c) can be obtained. The convex mirror provides a sizeable negative power to scatter the rays, while the concave mirror focuses rays and produces a greater angle of incidence in the focal plane. Compared to the above-mentioned structural forms, Fig. 1(c) shows it is easier to design a telescope with a large NA. In this configuration, unfortunately, the location of the stop is a serious problem, and there is no intermediate image plane. The telescope has no real entrance pupil, and stray light is grave.

2. Off-Axis Three-Mirror Telescope

Off-axis three-mirror telescopes are present in a variety of configurations. Among them, two structural forms shown in Fig. 2 and are widely used in the field of space remote sensing. Figure 2(a) shows the Cook structure form, and the stop can be located anywhere in the system. By adjusting the position of the stop, the telescope can be designed to be telecentric in the image space. The size of the telescope is compact, about 0.5–1 times the focal length. Yet, there is no intermediate image plane in this structural form. The ability to suppress stray light is weak.

Compared with the Cook telescope, the off-axis three-mirror telescope with an intermediate image plane has apparent

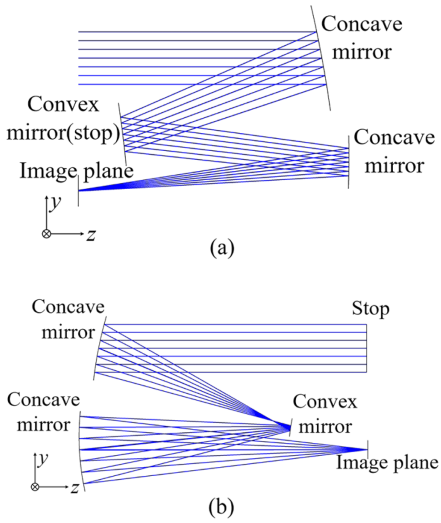

Fig. 2. Off-axis three-mirror telescope scheme of (a) Cook structure, (b) Korsch structure.

advantages in stray light suppression and alignment. In the last century, an off-axis three-mirror telescope with an intermediate image plane was presented, as shown in Fig. 2(b), which is called the Korsch telescope. In the Korsch telescope, the primary mirror and the tertiary mirror are concave mirrors, respectively, and the secondary mirror is convex. When the stop and the entrance pupil coincide in front of the primary mirror, the telescope has a real entrance pupil and can obtain the design result of the telecentric in the image space. The combination of the secondary and tertiary mirrors is similar to Fig. 2(b), which increases the incident angle of light at the focal plane to increase the NA of the telescope. This combination is not only found in the Korsch telescope, but also in extreme ultraviolet lithography objectives, where the last mirror group is mostly this combination. Just as a coin has two sides, the mirror group, which plays such an important role, not only provides convenience to the telescope but also brings some inevitable troubles. Due to the larger incident angle of the rays at the focal plane, the optics need a more significant amount of the decenter in the tangential direction, which makes the telescope have a large number of high-order aberrations that are difficult to correct.

3. Off-Axis Four-Mirror Telescope

The structures of the off-axis four-mirror telescope are legion, and it is difficult to introduce them in detail in this paper. In the off-axis four-mirror telescope, multiple optical elements allow for a more robust design potential of the system. According to the suitable combination of optical components, it is easier for the four-mirror telescope to meet the requirements of the intermediate image plane, the real entrance pupil, and the telecentric in the image space simultaneously.

It is generally accepted that the four-mirror telescope has longer focal lengths, a wider FoV, and larger NA. However, four-mirror telescopes require more space for installation, and more optical components make the telescope significantly more difficult to align and test. Therefore, in the design of most aerospace remote-sensing instruments, the designers still use the three-mirror telescope as much as possible or use some special

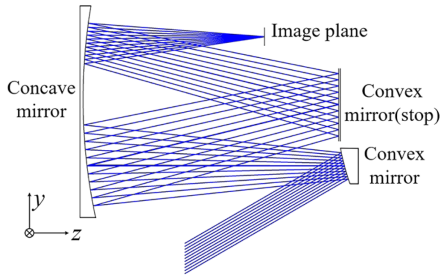

Fig. 3. Structure of the Seal telescope.

four-mirror telescope, such as the Seal telescope shown in Fig. 3, which has been successfully applied in GF-6 of China [8].

Based on the above comparative analysis of off-axis reflective telescopes with different structures, the following conclusions can be drawn:

(1) The two-mirror telescope has the advantages of simple structure and easy manufacture, and the technology is reliable and has been widely applied. Its disadvantage is that it is difficult to achieve the requirements of a wide FoV, large NA, and long focal length at the same time.
(2) The three-mirror telescope has the advantages of larger optical performance, various structural forms, a wide FoV, and long focal length. Its disadvantage is that it is more difficult to manufacture and align, and requires more design experience.
(3) The four-mirror telescope is an excellent scheme for ultralong focal length, ultrawide FoV, and ultralarge NA. Its disadvantage is that it is larger and has a more significant number of mirrors.

In this paper, the role of the telescope is mainly to collect the energy and information of the ground objects for the imaging spectrometer. The telescope has a one-dimensional FoV and is perpendicular to the direction of flight. Compared to other optical instruments, imaging spectrometers have lower light energy in a single channel and are easily affected by stray light. Therefore, stray light is strictly limited in imaging spectrometers. If the limitation of stray light can be implemented in the telescope, it will significantly reduce the design difficulty of the imaging spectrometer. The stop, the entrance or exit pupil, and the intermediate image plane of the telescope are the best positions that can reduce the impact of stray light on the system. Based on the unique design requirements, in the design of the telescope of the imaging spectrometer, we need to choose a structure with a real entrance or exit pupil and an intermediate image plane.

According to the characteristics of imaging spectrometer requirements, this paper gives a rough discussion and analysis of different forms of reflective telescopes. Two-mirror telescopes are difficult to meet complex design requirements, and four-mirror telescopes increase the complexity of the system. Undoubtedly, in three-mirror telescopes, the Korsch structure has excellent advantages in possessing a wide FoV and a large NA. And due to the presence of a real entrance pupil and the intermediate image plane, Korsch telescopes have significant advantages in stray light suppression and system alignment. Therefore, in this paper, we design a Korsch telescope for the imaging spectrometer.

B. Aperture Expansion Strategy of the Off-Axis Reflective Telescope with a Large NA

Compared with the off-axis optical system, the aberration theory and design method of the on-axis optical system are more perfect. Therefore, in the design of off-axis optical systems, designers prefer to use a convenient method to obtain initial structure parameters that satisfy aberration correction based on well-established on-axial aberration theory, and then proceed to off-axis design. When an immense value of the tilt or decenter is set, the on-axial structure parameters are severely broken. As a result, a gentle off-axis approach is widely used. The designer can shift the on-axial system to an off-axis system with a slow trend by increasing the value of the tilt or decenter in small increments, and eventually achieve a fully off-axis unobstructed design through several iterations. The method is effective most of the time, and the project of designing off-axis optical systems is made more accessible by using more efficient computers.

One such approach, however, is not always effective in the design of large NA off-axis reflective telescopes. In fact, the decenter and tilt of the optical elements are the most critical variables in each optimization iteration for the off-axis reflective telescope. The coupling properties exist between the decenter and tilt parameters of the optical component, due to the fact that we use an asymmetric optical element, which is the freeform surface. Furthermore, an optical component of the telescope with a large NA has a larger decenter or tilt value than a normal NA. As a result, when using the described design method, more iterative optimization processes are generated, which increases the probability that the optimization process will fall into a "local optimum." The design process of a large NA off-axis reflective telescope also requires the designer to have more design experience. To address this problem, in this paper, we present a design strategy applicable to the off-axis reflective telescope with a large NA, which is the aperture expansion. A detailed flow diagram of the aperture expansion strategy is shown in Fig. 4.

The design strategy for aperture expansion presented in this paper can be unfolded in detail and divided into two parts:

Part 1. The initial parameters of the off-axis telescope with a low NA. In this process, the designer first obtains the structural parameters of the on-axial telescope according to the geometric optical aberration theory. Then, based on the design experience, an off-axis telescope with a low NA was obtained, which could be used as the initial structure for the following segments. In this process of achieving an unobstructed low NA telescope, there is less variation in the positional parameters, such as the decenter or tilt of the optical elements. The design difficulty of the telescope is substantially reduced.

Part 2. Constraint construction and aperture expansion. In this process, based on the aperture expansion strategy, we increase the NA of the initial structure of the off-axis telescope. However, the direct result of increasing the NA is that light is obstructed by the optical element, and the image quality of the telescope is degraded, as shown in Fig. 5(a). Fortunately, following the above process (Part 1), the initial parameters of the

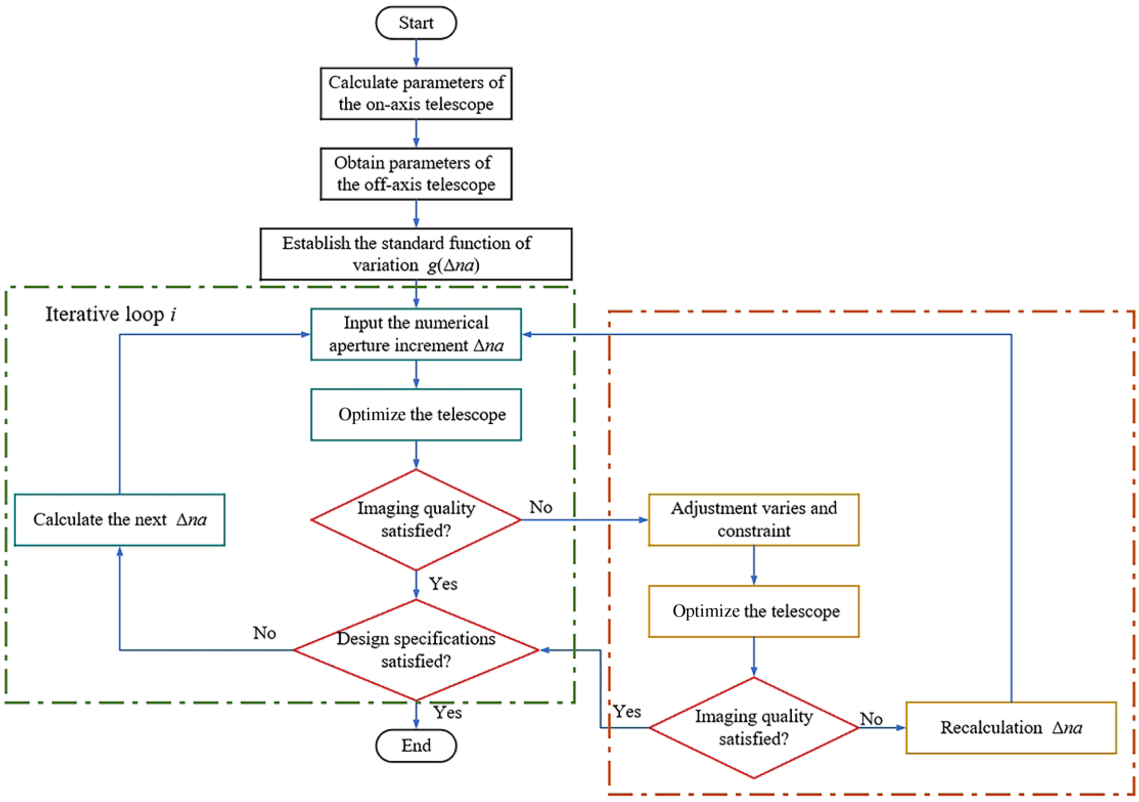

Fig. 4. Flow diagram of the aperture expansion strategy.

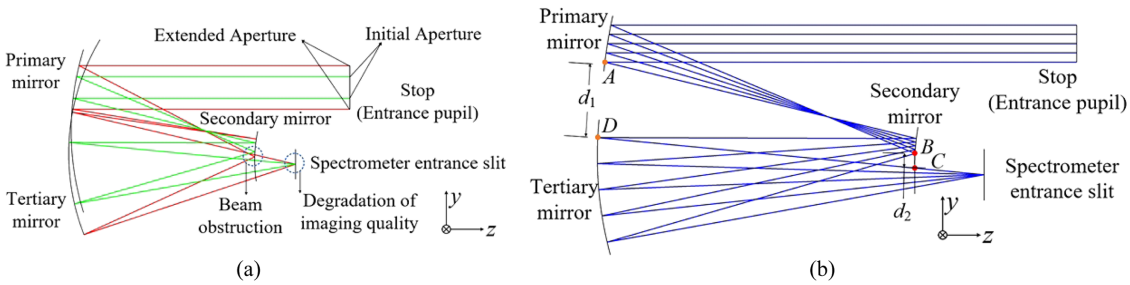

Fig. 5. (a) Beam obstruction in the process of the aperture expansion, and (b) the critical control points.

optical elements provide a better starting point for optimization in the obtained off-axis telescope initial structure with a low NA.

In addition, we need to place constraints on the position of the optical elements as much as constraints on the imaging quality. As shown in Fig. 5(b), A, B, C, and D are the critical control points, and d_1 and d_2 are the distances between control points A and D and between control points B and C, respectively. Their coordinates should satisfy Eq. (1),

$$\begin{cases} y_A > y_D \\ y_B > y_C \end{cases}. \tag{1}$$

In order for all the above constraints to be effectively controlled, we inevitably need to use aspherical surfaces in the design. When the aspherical surface also fails to meet the calibration requirements, as the NA increases, freeform surfaces will be used to obtain a better design result. Some researchers usually use multiple freeform surfaces in their designs and obtain better imaging quality. However, it is well known that using fewer freeform surfaces can significantly reduce the difficulty of testing, manufacturing, and alignment, although the result may not be comparable to the development with multiple freeform surfaces in terms of volume and imaging quality. However, there is still a huge improvement compared to spherical and aspherical surfaces. In our previous research, we compared the effects of using double freeform surfaces and a single freeform surface on the Offner imaging spectrometer. The results show that the size of the system is reduced by 37% in the single freeform surface design scheme. And the design result of double freeform surfaces is a 42% reduction in system size. It is clear that the result of the multiple freeform surface design does not change the system significantly compared to the single freeform surface design. As a result, considering that the two systems have many similar characteristics, in this paper, we have chosen to use a single freeform surface design scheme.

Based on the framework of nodal aberration theory, Fuerschbach *et al*. described the aberration field behavior

that emerges in optical systems with freeform optical surfaces [22,23]. In a classical Schmidt telescope, if the aspheric corrector plate is shifted longitudinally along the optical axis relative to the aperture stop, each field point receives a different contribution from the surface. This beam displacement results in a total surface aberration contribution $W_{\text{Correct, Notstop}}$, which is written as

$$W_{\text{Corrector, Notstop}} = W_{040}^{\text{asph}}[(\overrightarrow{\rho} + \Delta\overrightarrow{h})]^2, \tag{2}$$

where W_{040}^{asph} is the spherical aberration wave aberration contribution from the aspheric corrector plate, $\overrightarrow{\rho}$ is a normalized two-dimensional pupil vector, and $\Delta\overrightarrow{h}$ is the amount of relative beam displacement. If the freeform surface is located at the stop or pupil, the net aberration contribution of the freeform surface is field-constant. As the freeform optical surface is displaced away from the stop or pupil, the net aberration contribution becomes field-dependent.

Compared with the field aberration, the pupil aberration contributed by the large NA and the aberration in the tangential direction produced by the decenter or tilt of the optical element are the main aberrations of the telescope. In this telescope, the tertiary mirror is closer to the entrance pupil. On the tertiary mirror, the beams of different fields overlap significantly, but the diameter of the beam is larger, which facilitates the correction of pupil aberration through the freeform surface. Therefore, in this paper, the tertiary mirror is designed as a freeform mirror.

Based on the above analysis results and design method, we gradually increase the NA of the initial structure and iteratively optimize the optical system. However, the increase of the NA does not vary linearly. At the initial stage of aperture expansion, the system has relatively weak problems with beam obscuration and degradation of imaging quality even with a larger NA increase. As shown in Fig. 5(b), when the NA increases to larger values, beam obscuration and degradation of the imaging quality of the system can be a serious issue if the increment of the NA is constant. Therefore, the process of increasing the NA is nonlinear. In this paper, we establish the standard function of variation, $g(\Delta na)$, to evaluate the degree of beam obstruction and degradation of imaging quality with increasing NA, denoted as

$$g(\Delta na) = m\frac{f(B(\Delta na), C(\Delta na))}{f_{\min}(B, C)} + n\frac{h(\Delta na, c, l, k, a_i, d, t)}{h_{\min}}, \tag{3}$$

where Δna, c, l, k, a_i, d, and t are the NA increments, curvature, thickness, conic, and polynomial coefficients for aspheric or freeform surfaces, decenter, and tilt parameters, respectively. The functions of f and h are used to characterize the distance of the beam obstruction and the root mean square (RMS) radius of the spot after the degradation of the imaging quality, which can be accurately calculated by the ray-tracing algorithm based on the geometrical optics. $f_{\min}$ and $h_{\min}$ are the criteria for the distance of beam obstruction and the RMS radius of the spot after the degradation of the imaging quality. In addition, m and n are the weights for the distance of beam obstruction and the RMS radius of the spot after the degradation of the imaging quality, respectively.

In implementing the design flow shown in Fig. 4, it is necessary to first determine the standard function of variation $g(\Delta na)$ and set the values of the criteria $f_{\min}$ and $h_{\min}$.

If

$$\frac{f(B(\Delta na), C(\Delta na))}{f_{\min}(B, C)} > 1, \tag{4}$$

then $m = 0$; otherwise $m = 1$.

Similarly, if

$$\frac{h(\Delta na, c, l, k, a_i, d, t)}{h_{\min}} > 1, \tag{5}$$

then $n = 0$; otherwise $n = 1$.

In each cycle, the value of Δna is adjusted so that the right part of Eq. (3) is infinitely close to the $g(\Delta na)$. At this point, the Δna obtained is the amount of aperture expansion in the current cycle. According to Eqs. (3)–(5), the Δna is different in each cycle with a nonlinear variation. Next, based on the above design approach, we will design an off-axis reflective telescope of the imaging spectrometer with a wide FoV and large NA.

3. DESIGN EXAMPLE BASED ON THE APERTURE EXPANSION STRATEGY

Based on the detailed analysis of the foregoing, we calculated, in addition to the F-number parameter, the initial parameters of the telescope that satisfy the design specifications of Table 1. According to the classical aberration theory, the structural parameters of an on-axial telescope with a low NA are obtained. Then, depending on the results of some researchers, the off-axis parameters of the optical elements are further adjusted by the aperture off-axis method. As a result, we are able to obtain the initial structure of an off-axis telescope with a low NA, as shown in Fig. 6. The initial F-number of the telescope is set to 6. At this point, the control points A, B, C, and D do not have the problem of position mixing, and the control distances d_1 and d_2 are 80 and 25 mm, respectively. This result is sufficient to meet the design requirements of the unobstructed telescope. unobstructed.

Based on the design experience, when

$$f_{\min}(B, C) = 10 \text{ mm}, \quad \text{and } h_{\min} = 1.5 \times r_{\text{airy}}, \tag{6}$$

we consider the telescope to be adequate for both installation and image quality requirements, where r_{airy} is the Airy circle radius of the center wavelength. Obviously, in the initial few

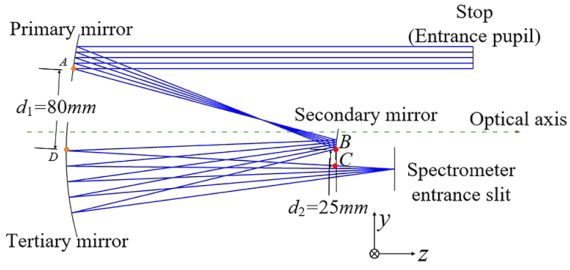

Fig. 6. Initial structure of the off-axis reflective telescope.

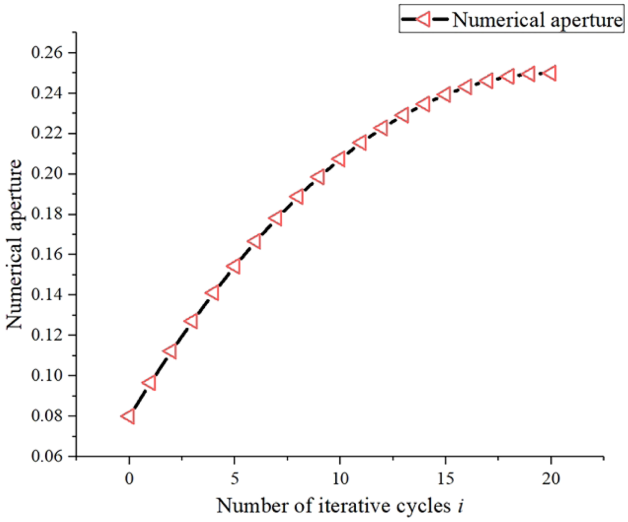

Fig. 7. Curve diagram of the aperture expansion path.

iterations, the parameter m in Eq. (3) is equal to 0. This indicates that the spatial constraint of the system will be reduced and the distance between the beam and the optical elements will remain within the minimum tolerance. With further aperture expansion, the advantage of spatial constraint will gradually disappear. At this point, the requirements of spatial constraints are significantly larger, and unobstructed light is a top priority for optimal design. According to Eq. (3), we determine the path of the aperture iteration; the curve of the aperture expansion path is shown in Fig. 7.

In Fig. 8, we show the four important nodes of the aperture expansion with F-numbers 2, 3, 4, and 5, respectively. As the NA varies, the image quality of the telescope also changes continuously. The RMS variation curve of these four nodes both before and after optimization is shown in Fig. 9. After each aperture adjustment, there is a significant increase in RMS, which is subsequently reduced by optimization. As the NA increases, the parameters of the optical elements are also changed, and the telescope shifts in a slow trend to a large NA design result. Such a design strategy is consistent with the design logic and does not suffer from the optimization problem of falling into a local optimum, which is one of the effective methods for large NA design.

The final design results obtained according to the aperture expansion strategy are shown in Fig. 10, and the overall size of the Korsch telescope with a freeform mirror is about 310 mm × 280 mm × 220 mm. The beam enters the system through the front aperture stop (entrance pupil), which has two unique advantages: 1) a significant reduction of stray light in the telescope; 2) a scanning mirror at the aperture stop, which can enhance the ability of the field coverage of the telescope. The beam is reflected by the primary mirror and then focused, and an intermediate image plane is generated between the primary mirror and the secondary mirror. In this position, we set the field-limiting aperture to eliminate stray light, which is formed by unexpected fields. Then, the beam is reflected by the secondary mirror and incident at a larger angle to the tertiary mirror. After being reflected by the tertiary mirror again, the beam passes through the exit pupil in front of the focal plane and is focused at a smaller angle. The incident angle of the chief rays in the focal plane for each field is shown in Fig. 11.

In the design, the primary and secondary mirrors are low-order aspheric mirrors, respectively, and the tertiary mirror is a freeform mirror that can be described by the xy polynomials [24]. The telescope is symmetric about the yoz plane, so the odd powers coefficients of x in the polynomials are zeros, and expression of the polynomials is

$$Z = \frac{cr^2}{1+\sqrt{1-(1+k)c^2r^2}} + p_0x^0y^1 + p_1x^2y^0 + p_2x^0y^2 + p_3x^2y^1 + p_4x^0y^3 + \cdots, \tag{7}$$

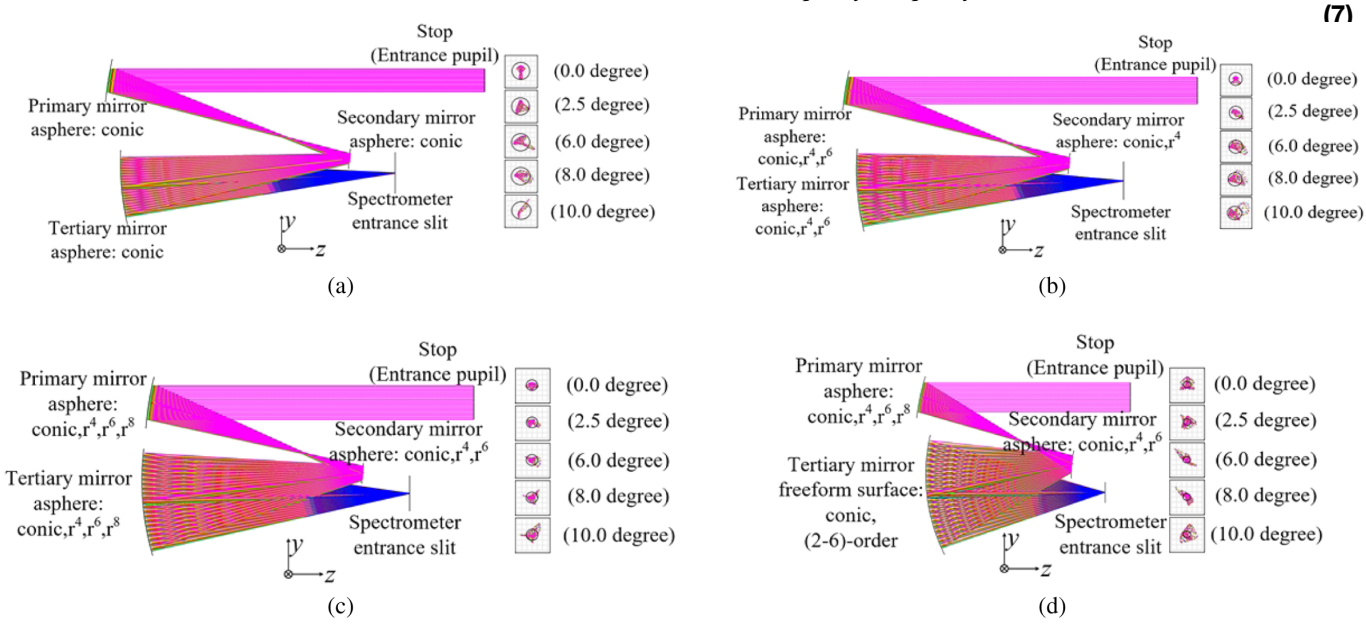

Fig. 8. Key nodes in the design of a large NA telescope based on aperture expansion strategy. (a) F-number of 5, (b) F-number of 4, (c) F-number of 3, (d) F-number of 2.

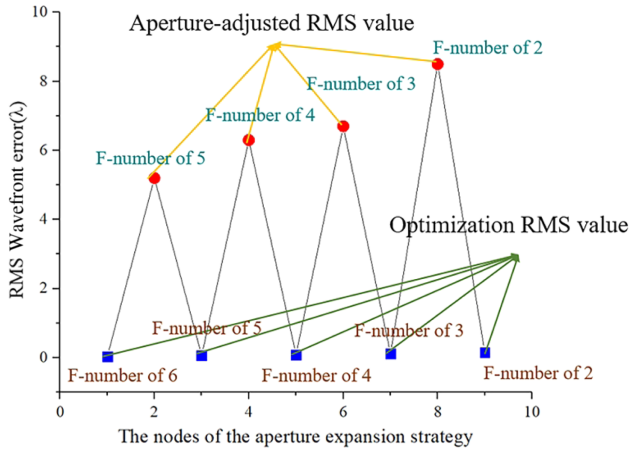

Fig. 9. RMS variation curve of the four important nodes.

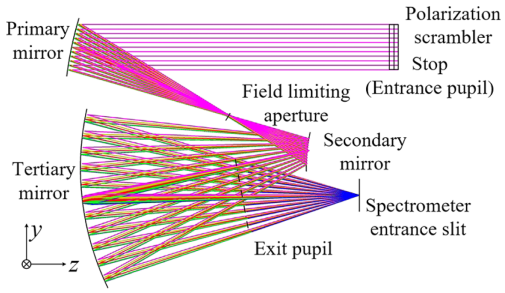

Fig. 10. Structure of the large NA telescope with a freeform mirror.

where c is the curvature, r is the radius, k is the quadratic coefficient, and p_i are the coefficients of the polynomials. The basic parameters of the telescope are shown in Table 2, and the coefficients of the aspheric mirror and freeform mirror are shown in Tables 3 and 4, respectively. The aperture of the freeform mirror is 200 mm × 200 mm, and the sag deviation of the freeform mirror after removing the best-fit sphere is shown in Fig. 12; the maximum sag deviation is 316 μm.

The spot diagram of the telescope is shown in Fig. 13, and all the RMS radii are smaller than the size of a single pixel. The modulation transfer function (MTF) of the overall spectrums of the telescope is shown in Fig. 14. The MTF at Nyquist frequency is larger than 0.62. The geometric-encircled energies are shown in Fig. 15, and all the energies are higher than 0.9. These indicate that the energy utilization of the spectrometer is high, which is helpful for improving the signal-to-noise ratio. And the distortion is less than 0.486%, as shown in Fig. 16. The telescope with a freeform mirror has a high performance.

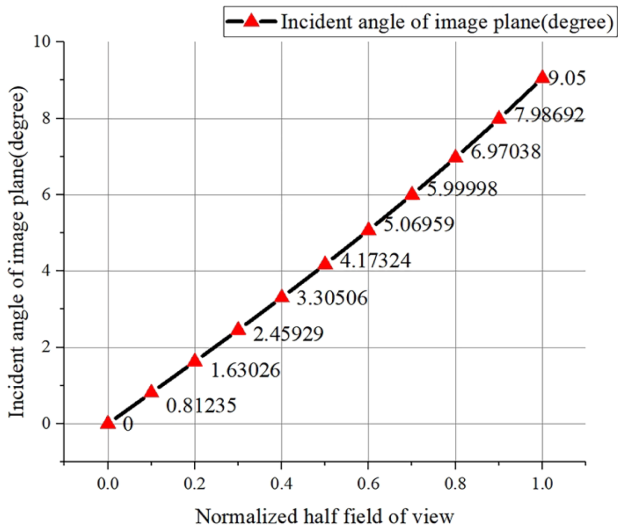

Fig. 11. Curve of the incident angle of chief rays in the focal plane.

Table 3. Aspherical Surface Coefficients of the Primary and Secondary Mirror

Term	Fourth Order	Sixth Order	Eighth Order
Primary mirror	–1.0859e-9	–4.8232e-15	1.2357e-19
Secondary mirror	1.8844e-7	2.5883e-11	-

Table 4. Freeform Surface Coefficients of the Tertiary Mirror

Term	Coefficient ai	Term	Coefficient ai	Term	Coefficient ai
x^2y^0	–1.2209e-5	x^2y^2	–6.3406e-11	x^6y^0	4.4684e-15
x^0y^2	–1.0003e-5	x^0y^4	–5.1738e-10	x^4y^2	–3.0916e-16
x^2y^1	1.0671e-7	x^4y^1	1.1337e-12	x^2y^4	–1.1085e-14
x^0y^3	5.1638e-8	x^2y^3	–1.4203e-12	x^0y^6	–9.0185e-15
x^4y^0	1.2175e-10	x^0y^5	–2.9423e-12	-	-

Tolerance analysis is an essential step in optical design, which must be done to investigate the impact of misalignments and errors during fabrication of the system. It is also a key step in assessing optical instrument manufacturability. In the tolerance analysis, the criterion of MTF degradation is accepted as 0.2. We have listed eight factors that have a significant impact on the telescope at the all-spectrum range in Table 5. All tolerance values are obtained after 500 Monte Carlo simulation runs.

Table 2. Basic Parameters of the Telescope

Surface	Surface Type	Radius (mm)	Thickness (mm)	Material	Tilt Angle (deg)
1	Object plane	-	-	-	0
2	Stop	-	–310	-	0
3	Primary mirror	312.099	225.217	mirror	0
4	Secondary mirror	186.146	–200.217	mirror	–4.142
5	Tertiary mirror	252.300	248.968	mirror	16.156
6	image plane	-	-	-	0

Moreover, the given tolerance values conform to the manufacturing technology. The RMS of the primary mirror surface irregularity is better than $\lambda/40$ ($\lambda = 632.8$ nm), and the RMSs of the secondary mirror and tertiary mirror surface irregularity are better than $\lambda/30$. The result shows a 90% probability that the MTF only changed by 0.1. The simulation results are shown in Fig. 17. The telescope used in our design is feasible for fabrication and alignment.

4. CONCLUSION

In this paper, the structural forms of off-axis reflective telescopes are analyzed according to the unique requirements of the hyperspectral imaging spectrometer for the monitoring of

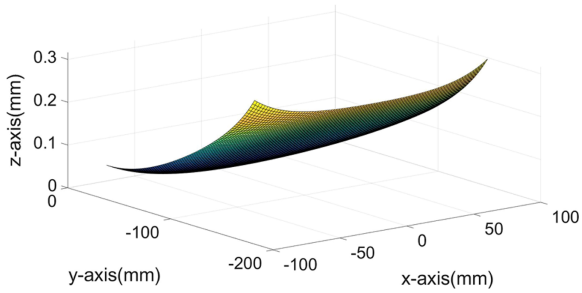

Fig. 12. Schematic diagram of the sag deviation.

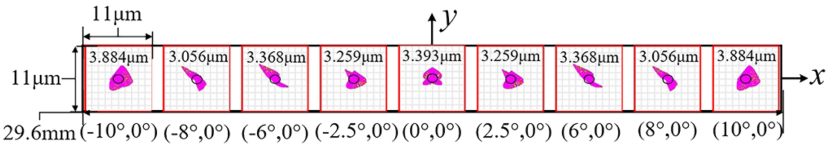

Fig. 13. Spot diagram of the telescope.

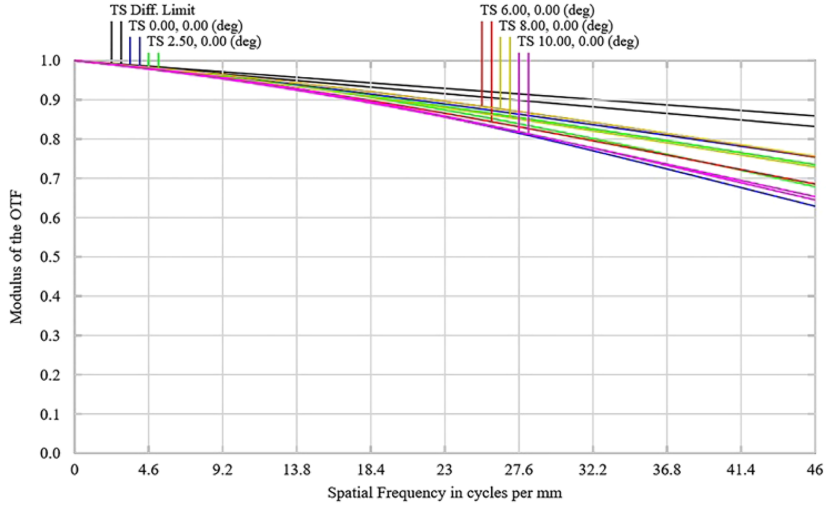

Fig. 14. MTF of the telescope.

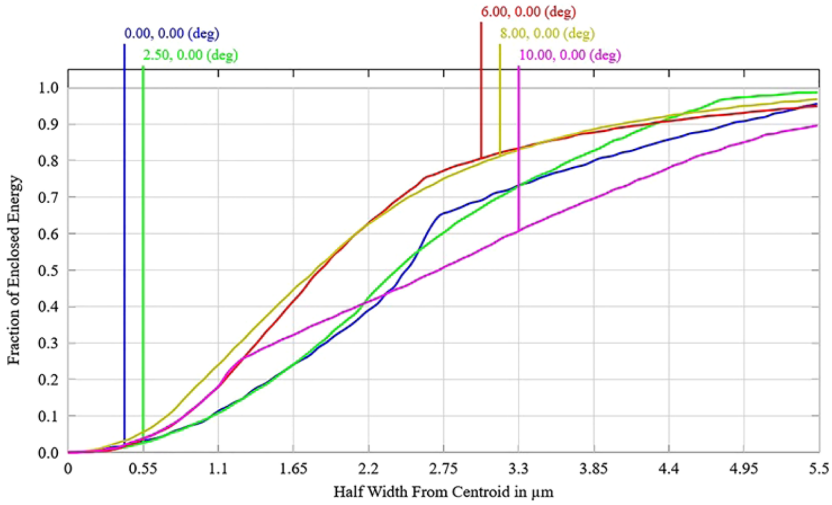

Fig. 15. Geometric-encircled energies of the telescope.

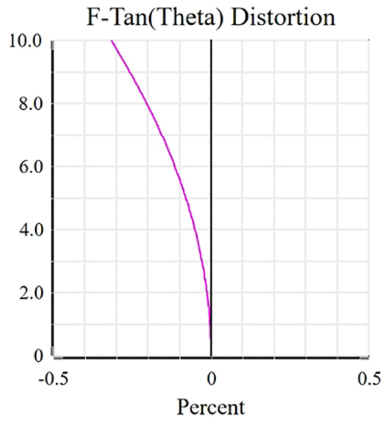

Fig. 16. Distortion curve of the telesope.

greenhouse gas. As a result, we chose the Korsch telescope to obtain the design results of a telescope with a wide FoV, a large NA, and low stray light for the imaging spectrometer. Then, we present a design method for a large NA telescope with a freeform mirror based on the aperture expansion strategy. Based on this method, we designed a telescope with a focal length of 84 mm, an F-number of 2, and an FoV of 20°. The analysis of the image quality shows that the telescope is high performance and satisfies the requirements of the design specifications. The freeform mirror meets current machining capability, and the designed telescope has a feasible manufacturing capability. The aperture expansion strategy is effective and practical for creating off-axis reflective telescopes with a large NA. The design methods and results presented in this paper will contribute to the development of a new generation of global greenhouse gas monitoring instruments.

Table 5. Tolerance Analysis of the Telescope

Tolerance Items	Element	Given Value	Change of MTF
Element x-decenter (mm)	tertiary mirror	–0.015	0.044
Element x-decenter (mm)	primary mirror	0.015	0.041
Element y-tilt (deg)	tertiary mirror	0.01	0.041
Element y-tilt (deg)	primary mirror	–0.01	0.037
Element y-decenter (mm)	secondary mirror	0.01	0.024
Element y-decenter (mm)	primary mirror	0.015	0.019
Element x-tilt (degree)	primary mirror	0.01	0.018
Element y-decenter (mm)	tertiary mirror	–0.015	0.015

Funding. National Key Research and Development Program of China (2021YFB3901000).

Disclosures. The authors declare that they have no conflicts of interest related to this paper.

Data availability. The data that support the findings of this study are available from the authors upon reasonable request.

REFERENCES

1. B. Sierk, V. Fernandez, J. L. Bezy, Y. Meijer, Y. Durand, G. Lacoste, C. Pachot, A. Loscher, H. Nett, K. Minoglou, L. Boucher, R. Windpassinger, A. Pasquet, D. Serre, and F. Hennepe, "The Copernicus CO_2M mission for monitoring anthropogenic carbon dioxide emissions from space," Proc. SPIE **11852**, 1188523M (2021).
2. R. R. Basilio, H. R. Pollock, and S. L. Hunyadi-Lay, "OCO-2 (Orbiting Carbon Observatory-2) mission operations planning and initial operations experiences," Proc. SPIE **9241**, 924105 (2014).
3. A. Eldering, T. E. Taylor, C. W. O'Dell, and R. Pavlick, "The OCO-3 mission; measurement objectives and expected performance based on one year of simulated data," Atmos. Meas. Tech. **12**, 2341–2370 (2019).
4. R. Geyl, E. Ruch, R. Bourgois, R. M. Ythier, H. Leplan, and F. Riguet, "Thermal and near-infrared sensor for carbon observation Fourier transform spectrometer-2 (TANSO-FTS-2) on the Greenhouse gases Observing SATellite-2 (GOSAT-2) during its first year in orbit," Atmos. Meas. Tech. **14**, 2013–2039 (2021).
5. D. Yang, Y. Liu, H. Boesch, L. Yao, A. D. Noia, Z. Cai, N. Lu, D. Lyu, M. Wang, J. Wang, Z. Yin, and Y. Zheng, "A new TanSat XCO_2 global product towards climate studies," Adv. Atmos. Sci. **38**, 8–11 (2021).

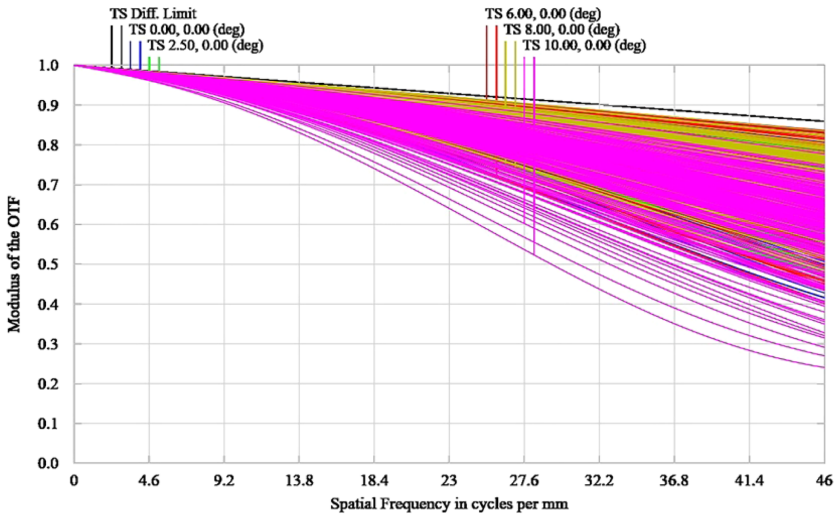

Fig. 17. Tolerance simulation results of Monte Carlo simulation.

6. D. Nijkerk, B. Venrooy, P. Doorn, R. Henselmans, F. Draaisma, and A. Hoogstrate, "The TROPOMI telescope," Proc. SPIE **10564**, 105640Z (2017).
7. M. Beier, J. Hartung, T. Peschel, C. Damm, A. Gebhardt, S. Scheiding, D. Stumpf, U. Zeitner, S. Risse, R. Eberhardt, and A. Tunnermann, "Development, fabrication, and testing of an anamorphic imaging snap-together freeform telescope," Appl. Opt. **54**, 3530–3542 (2015).
8. X. Zhang, L. Zheng, X. He, L. Wang, F. Zhang, S. Yu, G. Shi, B. Zhang, Q. Liu, and T. Wang, "Design and fabrication of imaging optical systems with freeform surfaces," Proc. SPIE **8486**, 848607 (2012).
9. J. Reimers, A. Bauer, K. P. Thompson, and J. P. Rolland, "Freeform spectrometer enabling increased compactness," Light Sci. Appl. **6**, e17026 (2017).
10. T. Yang, D. Cheng, and Y. Wang, "Freeform imaging spectrometer using a point-by-point design method," Appl. Opt. **57**, 4718–4727 (2018).
11. J. Zhu, T. Yang, and G. Jin, "Design method of surface contour for a freeform lens with wide linear field-of-view," Opt. Express **21**, 26080–26092 (2013).
12. J. Zhu, X. Wu, T. Yang, and G. Jin, "Generating optical freeform surfaces considering both coordinates and normals of discrete data points," J. Opt. Soc. Am. A **31**, 2401–2408 (2014).
13. T. Yang, G. Jin, and J. Zhu, "Automated design of freeform imaging systems," Light Sci. Appl. **6**, e17081 (2017).
14. J. P. Rolland, M. A. Davies, T. J. Suleski, C. Evans, A. Bauer, J. C. Lambropoulos, and K. Falaggis, "Freeform optics for imaging," Optica **8**, 161–176 (2021).
15. R. Geyl, E. Ruch, R. Bourgois, R. Mercier-Ythier, H. Leplan, and F. Riguet, "Freeform optics design, fabrication, testing technologies for space applications," Proc. SPIE **11180**, 111800P (2019).
16. Q. Meng, H. Wang, W. Liang, Z. Yan, and B. Wang, "Design of off-axis three-mirror systems with ultrawide field of view based on an expansion process of surface freeform and field of view," Appl. Opt. **58**, 609–615 (2019).
17. D. Korsch, "Wide-field three-mirror collimator," U.S. patent 4,737,021 A (12 April 1986).
18. L. G. Cook and J. F. Silny, "Imaging spectrometer trade studies: a detailed comparison of the Offner-Chrisp and reflective triplet optical design forms," Proc. SPIE **7813**, 78130F (2010).
19. L. G. Cook, "Method and apparatus for receiving optical signals," U.S. patent 4,834,517 A (30 May 1989).
20. J. L. Bezy, V. Fernandez, B. Sierk, A. Loscher, H. Nett, and Y. Meijer, "The European Copernicus mission for anthropogenic CO_2 emission monitoring," Proc. SPIE **11501**, 1150103 (2020).
21. J. Zhang, Y. Zheng, C. Lin, Z. Ji, and H. Wu, "Analysis method of the Offner hyperspectral imaging spectrometer based on vector aberration theory," Appl. Opt. **60**, 264–275 (2021).
22. K. Fuerschbach, J. P. Rolland, and K. P. Thompson, "Extending nodal aberration theory to include mount-induced aberrations with application to freeform surfaces," Opt. Express **20**, 20139–20155 (2012).
23. K. Fuerschbach, J. P. Rolland, and K. P. Thompson, "Theory of aberration fields for general optical systems with freeform surfaces," Opt. Express **22**, 26585–26606 (2014).
24. J. Zhang, C. Lin, Z. Ji, H. Wu, C. Li, B. Du, and Y. Zheng, "Design of a compact hyperspectral imaging spectrometer with freeform surface based on anastigmatism," Appl. Opt. **59**, 1715–1725 (2020).